Advances in Geo-Energy Research

Vol. 19, No. 3, p. 231-241, 2026

Original article

Multifunctional nanofluids for enhanced oil recovery by simultaneous *in situ* mobility control and displacement efficiency improvement

Mkhitar Ovsepian[1], Yusuff Salami[1], Tagir Karamov[1], Daijun Du[2], Ilya Dobysh[3], Alexey Cheremisin[1,3], Chengdong Yuan[1]*

[1]*Center for Petroleum Science and Engineering, Skolkovo Institute of Science and Technology, Moscow 121205, Russia*

[2]*State Key Laboratory of Oil and Gas Reservoir Geology and Exploitation, Southwest Petroleum University, Chengdu 610500, P. R. China*

[3]*LABADVANCE LLC, Moscow 121205, Russia*

Keywords:
Chemical enhanced oil recovery
emulsion flooding
microemulsions
nanoparticles
emulsion stability

Cited as:
Ovsepian, M., Salami, Y., Karamov, T., Du, D., Dobysh, I., Cheremisin, A., Yuan, C. Multifunctional nanofluids for enhanced oil recovery by simultaneous *in situ* mobility control and displacement efficiency improvement. Advances in Geo-Energy Research, 2026, 19(3): 231-241.
https://doi.org/10.46690/ager.2026.03.03

Abstract:
Compared with conventional chemical enhanced oil recovery methods, micro/nanofluid-based emulsion systems offer several advantages, including improved mobility control, enhanced stability, and effective modification of interfacial properties, while requiring lower chemical dosage and exhibiting better tolerance to harsh reservoir conditions. This study systematically evaluated the potential of a novel nanofluid-based emulsion as an enhanced oil recovery agent, with emphasis on its rheological behavior, emulsion stability, and interfacial performance. Rheological measurements demonstrate that emulsion viscosity is strongly influenced by the water-to-oil ratio and mixing duration. Systems with low oil content exhibit only modest viscosity changes, whereas increasing oil fraction and mixing time result in pronounced viscosity enhancement, indicating the formation of structured emulsion networks. This viscosity growth contributes to improved emulsion stability, which is further supported by microscopic observations revealing complex multiphase structures. Interfacial characterization shows that the nanofluid-based emulsion effectively lowers the oil-water interfacial tension and induces a strong wettability shift toward water-wet conditions, both of which are favorable for enhanced oil displacement. Microfluidic displacement experiments provide pore-scale evidence that the combined effects of viscosity enhancement, improved emulsion stability, interfacial tension reduction, and wettability alteration lead to efficient mobilization of residual oil. Visual observations confirm *in situ* emulsion formation within the porous network and improved sweep behavior compared with conventional water injection. Overall, the results highlight the multifunctional role of nanofluid-based emulsions in stabilizing flow, enhancing sweep efficiency, and modifying interfacial dynamics, demonstrating their strong potential as an advanced chemical strategy for enhanced oil recovery applications.

1. Introduction

As global energy demand continues to rise and easily recoverable oil reserves become more limited, there is a growing need to explore more efficient and sustainable technologies for the development of oil and gas reservoirs. Among the various enhanced oil recovery (EOR) techniques, chemical EOR (cEOR) methods have shown promising results by improving sweep efficiency, microscopic displacement efficiency, or both (Shakeel et al., 2024; Liu et al., 2025). Various cEOR methods

Yandy Scientific Press

*Corresponding author.
E-mail address: Mkhitar.Ovsepian@skoltech.ru (M. Ovsepian); vonuseful@vk.com (Y. Salami); T.Karamov@skoltech.ru (T. Karamov); axiaodu1991@163.com (D. Du); dobysh@labadvance.net (I. Dobysh); A.Cheremisin@skoltech.ru (A. Cheremisin).
2207-9963
Received December 3, 2025; revised January 16, 2026; accepted February 10, 2026; available online February 13, 2026.

have been studied for application in different reservoir types, including surfactant flooding, polymer flooding, alkaline-surfactant-polymer flooding, and foam injection. Surfactant flooding reduces the interfacial tension (IFT) between oil and water and can alter rock wettability from oil-wet to water-wet, while polymer flooding increases the viscosity of the injected water to improve sweep efficiency by mitigating viscous fingering and channeling in high-permeability zones. Surfactant-polymer or alkaline-surfactant-polymer technologies combine the synergistic effects of IFT reduction, wettability alteration, and mobility control, thereby offering significant potential for EOR. However, the performance of these chemical methods is often compromised by harsh reservoir conditions (such as high salinity, high temperature, and strong adsorption of chemicals onto the rock surface), which can affect the stability and efficiency of the injected agents, while their field application also requires specialized injection units and additional surface facilities, further increasing operational complexity and cost. To address these challenges, emulsions have been proposed as an alternative cEOR approach (Karambeigi et al., 2015; Pu et al., 2025). They can be prepared externally or formed dynamically within the reservoir using natural surfactants, added emulsifiers, or alkaline agents that reduce IFT and stabilize the emulsion, improving sweep efficiency, particularly in heavy oil recovery (Yang et al., 2024). In this work, nanotechnology has emerged as a powerful tool to overcome the limitations of traditional cEOR agents by further enhancing emulsion stability, adaptability, and performance under harsh reservoir conditions (Behera et al., 2024).

Despite the wide variety of nanoparticles (NPs) studied for EOR applications, this paper specifically focuses on nanofluids (NFs) which are stable suspensions of NPs dispersed in base fluids such as water or brine. Alnarabiji et al. (2018) reported that a 0.01% zinc oxide nanocrystal (ZnO-NC) nanofluid achieved up to 50% oil recovery. Jang and Lee (2024) demonstrated that surface-modified silica NFs in high-salinity carbonate reservoirs moderately reduced IFT (5-10 mN/m) and decreased the contact angle (CA) by 62.8%, indicating a shift toward a more water-wet surface, while *in situ* emulsions enhanced sweep efficiency and reduced viscous fingering, resulting in a 20% improvement in recovery over waterflooding. Emulsions, which are thermodynamically stable dispersions of two immiscible liquids, effectively penetrate tight pores, stabilize oil-water interfaces, and improve mobility control, making them promising for EOR, particularly in heavy oil reservoirs (Wu et al., 2024). Gong et al. (2022) showed that alkali-silica nanoparticle-polymer stabilized emulsions altered wettability and improved sweep efficiency, achieving a 21.05% increase in oil recovery. Pang et al. (2024) demonstrated that amphiphilic montmorillonite-based NFs formed stable W/O emulsions at low NP concentrations (0.1 wt%) and high water-to-oil ratio (WOR) (80%), increasing apparent viscosity and improving recovery by 14.88% compared to brine, mainly through wettability alteration and enhanced conformance control.

In the present study, the specific surface modification strategy for SiO_2 NPs was selected based on insights from the work by Du et al. (2026), where molecular simulations identified the most effective functional groups for enhancing nanoparticle stability and interfacial activity under harsh reservoir conditions. Despite the promising advantages of nano-cEOR, its practical application still faces key challenges, including nanoparticle aggregation under reservoir conditions, retention or plugging in porous media, high synthesis costs, and limited field-scale demonstrations. Moreover, most existing studies are focused on either an individual mechanism (e.g., IFT reduction, wettability alteration, or viscosity enhancement) or specific reservoir types, while the combined pore-scale effects of nanofluid-stabilized emulsions, particularly their roles in mobility control, stability, viscosity enhancement, and *in situ* emulsification under reservoir-relevant conditions, remain insufficiently understood. These gaps motivate the present study, which systematically investigates the synergistic effects of nanofluid-based emulsions using rheological, interfacial, and microfluidic analyses to provide new insights into their EOR potential and practical applicability.

Microfluidic technology, which has recently emerged as a powerful tool for studying EOR processes at the pore scale, enables fast, cost-effective, and visually observable displacement experiments that replicate complex reservoir structures (Lu et al., 2025). Beyond traditional core flooding, this method allows direct visualization of both microscopic sweep and displacement efficiencies, providing unique insights into pore-scale fluid interactions. While it has been successfully applied to polymers, surfactants, alkali-surfactant-polymer systems, NFs, and foams, its use for directly observing *in situ* emulsion formation has not yet been explored. This work therefore provides novel insights into the dynamic behavior of NF-stabilized emulsions and their synergistic EOR mechanisms, offering valuable guidance for upscaling and potential field application.

2. Materials and methods

2.1 Materials

The crude oil sample used in this study was obtained from the West Siberia Basin. Prior to experiments, the oil was dehydrated using calcium chloride and centrifugation to reduce the water content to less than 0.01 wt%. This crude oil was used in all IFT, wettability, emulsion, and microfluidic experiments to evaluate the performance of the NF. At the reservoir temperature of 40 °C, crude oil exhibited a density of 0.934 g/cm^3 and a viscosity of 67.12 mPa·s, with an average molecular weight of 309 g/mol. The synthetic brine used in the experiments had a density of 1.0043 g/cm^3, a viscosity of 0.679 mPa·s, and a total salinity of 17,383.4 mg/L. The NF in this study was prepared as concentrated dispersions containing 35 wt% commercially available SiO_2 NPs, an AEC anionic surfactant, and nano-crystalline cellulose. The NPs were initially dispersed in deionized water with surfactant assistance to enhance colloidal stability and prevent aggregation. This dispersion was achieved using an overhead stirrer at 500 rpm for 30 minutes, followed by ultrasonication for 30 minutes to ensure a uniform and stable suspension. Prior to experiments, the nanofluid concentrate was diluted in synthetic brine to the desired working concentrations. The carbonate rock samples

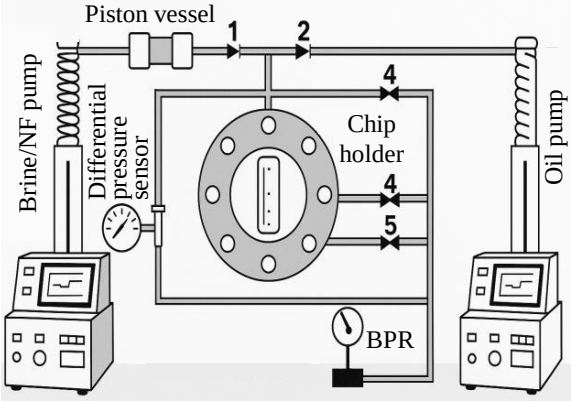

Fig. 1. Schematic representation of the microfluidic assembly.

used in this study were selected to represent typical reservoir conditions in oil-bearing carbonate formations. The core plug was cylindrical in shape, with a diameter of 3 cm and a length of approximately 6 cm. The mineralogical composition was primarily calcite, confirmed by X-ray diffraction.

2.2 Nanoparticle characterization

The morphology and particle size of the modified SiO_2 NPs were investigated using scanning electron microscopy (SEM) on a Quattro S ESEM system (Thermo Fisher Scientific, USA). The analysis was performed at an accelerating voltage of 10 kV and 0.83 nA current, utilizing both secondary electron and backscattered electron detectors to obtain information on surface topography and compositional contrast, respectively. A small droplet of the NF solution was deposited on a clean steel stub and dried at 70°C without applying any conductive coating. For particle size distribution in suspension, dynamic light scattering (DLS) analysis was performed using a Zetasizer Nano ZS (Malvern Panalytical, UK).

2.3 Emulsion preparation and characterization

Emulsions were prepared by mixing crude oil with a 0.3 wt% aqueous NF solution at predefined WORs, ranging from 50:50 to 80:20 by volume. The NF solution and crude oil were combined in 50 mL glass cylinders specially designed for this purpose. An overhead stirrer EUROSTAR 40 (IKA, USA) equipped with a custom 3D-printed propeller was used to ensure efficient mixing without contacting the cylinder walls. The propeller was positioned at the interface between the two phases to optimize mixing efficiency and promote uniform emulsion formation. Emulsification was conducted at 1,000-2,000 rpm for 2 h to produce a stable emulsion. The morphological characteristics and droplet size distribution of the prepared emulsions were investigated using a Carl Zeiss AxioScope 5 optical microscope (Carl Zeiss AG, Germany). Sample preparation involved placing an aliquot of approximately 5 μL of the emulsion onto a standard glass microscope slide, which was then carefully covered with a coverslip to minimize sample distortion. Digital micrographs were captured in bright-field transmission mode using 10× and 40× objectives. Optical microscopy images of the emulsions were captured and analyzed using ImageJ (National Institutes of Health, USA), which enabled precise measurement of droplet size and size distributions by processing multiple regions of interest.

2.4 Contact angle and IFT measurements

Contact angle measurements were performed using a DSA100S (KRUSS, Germany) to evaluate wettability changes on carbonate rock surfaces. Polished discs were first analyzed to determine native wettability, then cleaned via Soxhlet extraction with toluene and dried at 90 °C for 24 h. To mimic oil-wet conditions, samples were aged in crude oil at 70 °C for 72 h. Afterward, they were exposed to NF at 40 °C, with CA measured over time using the sessile drop method and brine as the probe fluid. All measurements were performed at ambient conditions, with images analyzed via ADVANCE software (KRUSS, Germany), averaging results from multiple spots. IFT was measured using an SDT (KRUSS, Germany) with the spinning drop method to evaluate crude oil - NF interfacial behavior. A crude oil droplet was injected into a NF-filled capillary and rotated at 3,000-5,000 rpm. The IFT was determined by analyzing the equilibrium shape of the spinning oil droplet using the Vonnegut equation (for low IFT values) or the Laplace equation (for high IFT values), depending on the droplet profile.

2.5 Rheological measurements

The apparent viscosity was measured using a Brookfield DV2TLV rotational viscometer (AMETEK Brookfield, USA) at 40°C. Fluids were carefully loaded into the sample chamber to minimize air entrapment and avoid phase separation. Viscosity readings were recorded once stable values were achieved to ensure measurement reliability and repeatability. In addition to viscosity, rheological properties such as shear rate and shear stress were also measured to evaluate the flow behavior of the nanofluid solution.

2.6 Microfluidic displacement tests

Microfluidic tests were performed using a custom-built setup capable of operating at high pressure (up to 60 MPa) and high temperature (up to 250 °C). The system includes a microfluidic chip holder, dual plunger pumps, hydraulic valves, a back-pressure regulator (BPR), insertion heaters regulated by a thermocouple, and differential pressure sensors. The entire setup is managed via a special control unit and PC interface. A schematic of the setup is provided in Fig. 1, while a more detailed description of the experimental system is available in the literature (Dorhjie et al., 2024).

The workflow consisted of several steps: (1) Assembling the platform by sealing the microfluidic chip with sapphire glass between stainless steel plates; (2) Preparing the pumps and connecting hydraulic lines; (3) Vacuuming and heating the system to 40 °C, followed by pressurization to 11.2 MPa using crude oil to fully saturate the chip; (4) Injecting brine through the bypass and then through the chip at low rates (0.0003-0.07 mL/min) until no further oil was produced, followed by NF solution injection under the same flow conditions; (5) Monitoring fluid displacement via UV-illuminated microscopy, leveraging the natural fluorescence of crude oil. Video data

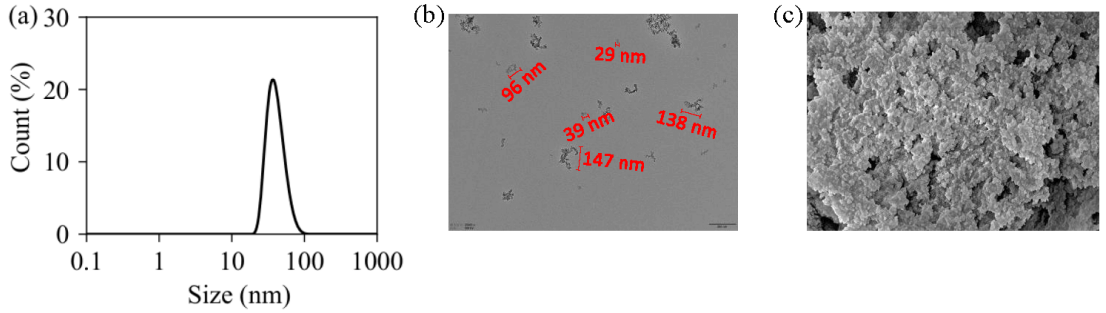

Fig. 2. NP characterization: (a) DLS particle size distribution and (b)-(c) SEM micrographs illustrating particle morphology and size.

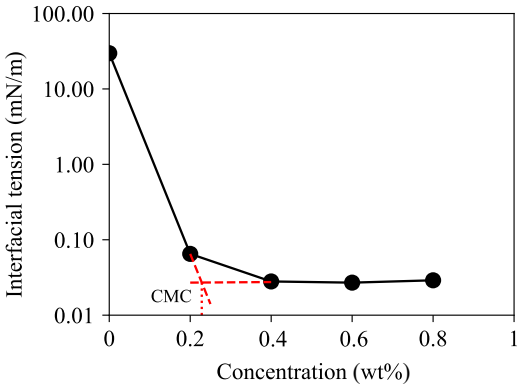

Fig. 3. Effect of NF concentration on IFT.

were processed using Python (version 3.11.5). Preprocessing included contrast enhancement and grayscale conversion, followed by testing multiple binarization algorithms (global thresholding, adaptive mean, and Otsu's method). The algorithm offering the best segmentation accuracy was selected for further recovery factor analysis.

3. Results and discussion

3.1 Physicochemical characterization of nanofluid systems

To evaluate the dispersion characteristics of the prepared NF, DLS measurements were performed. As shown in Fig. 2(a), the mean hydrodynamic diameter was approximately 37.8 nm. The relatively high polydispersity index (PDI) indicates the presence of some aggregates, likely associated with the natural polymer-based modifier. In contrast, SEM analysis (Figs. 2(b)-2(c)) showed that individual NPs fall within the 30-70 nm range, while clustered structures may reach up to 150 nm, confirming the coexistence of discrete particles and polymer-induced clusters.

The discrepancy between DLS and SEM results arise from their different measurement principles. DLS measures the hydrodynamic diameter of NPs in suspension, which captures not only the solid particle but also solvation layers and surface-bound polymer chains. Thus, even with a modest mean size, an elevated PDI reflects the presence of a fraction of larger aggregates (Souza et al., 2016). SEM, on the other hand, provides direct visualization of the dried NPs, enabling clear differentiation between individual particles and clusters. Consequently, SEM reports the actual particle size range (30-70 nm) and cluster dimensions (up to 150 nm), whereas DLS reflects the averaged dynamic behavior in liquid, making the observed differences between the two methods expected (Filippov et al., 2023; Sepahvand et al., 2024).

The stability of the prepared NF systems was evaluated through visual observation over a 45-day period for three different concentrations: 0.3, 0.6, and 1.0 wt%. All dispersions appeared homogeneous after preparation, but noticeable sedimentation and nanoparticle precipitation were observed after approximately two weeks, along with surfactant separation forming a thin layer at the air-brine interface. This indicates possible oversaturation and reduced colloidal stability due to surfactant depletion from particle surfaces or ionic interactions in the brine. Nevertheless, mild agitation was sufficient to redisperse the particles, and all samples regained a uniform appearance, suggesting reversible aggregation.

3.2 IFT measurements

The effect of NF concentration on IFT was examined in the range of 0.2 and 0.8 wt% (Fig. 3). Compared to the initial IFT of 29.77 mN/m for pure brine, all NF formulations showed a significant reduction. IFT values steadily decreased up to approximately 0.3-0.4 wt%, after which the reduction plateaued, indicating interfacial saturation. This suggests that the system approaches its critical micelle concentration around 0.23 wt%, beyond which further increase in concentration does not significantly enhance interfacial activity and may lead to NP clustering or reduced stability. Therefore, 0.3 wt% was selected as an optimal concentration for further experiments, ensuring effective IFT reduction without compromising NF stability.

The effect of brine salinity on IFT was investigated over a range of 18 to 200 g/L at a fixed NF concentration of 0.3 wt%. As shown in Fig. 4, the lowest IFT (0.0288 mN/m) was observed at 18 g/L, which corresponds to the target reservoir salinity, indicating highly effective interfacial activity of the silica-based NF. This behavior is consistent with previous reports showing that silica NFs exhibit optimal IFT reduction and EOR under low-salinity conditions (Mansouri Zadeh et al., 2024). Moderate salinity levels (40-80 g/L) resulted in only a slight increase in IFT (0.042-0.044 mN/m), whereas a

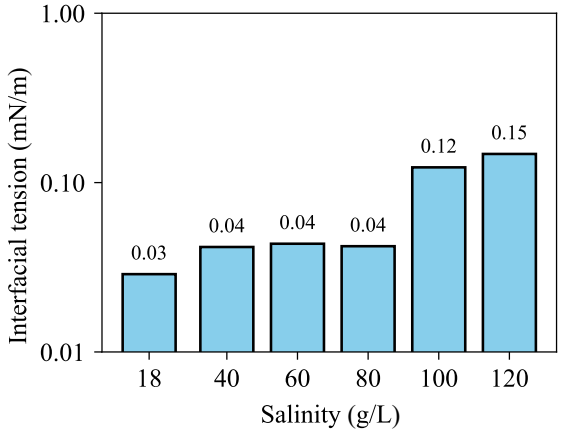

Fig. 4. Effect of brine salinity concentration on IFT.

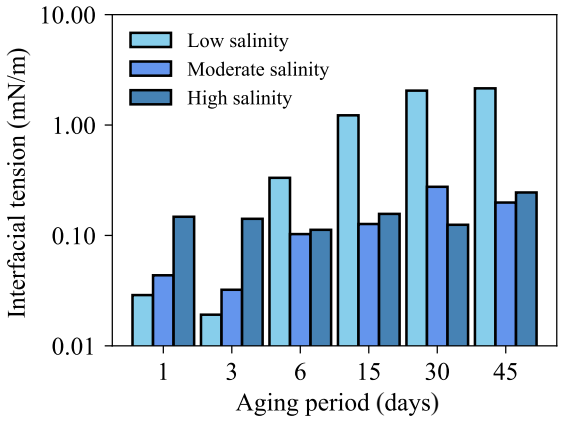

Fig. 5. Effect of aging time on NF interfacial performance at different salinities.

pronounced rise was observed at high salinities of 100 and 200 g/L, with IFT values reaching 0.123 and 0.148 mN/m, respectively.

The salinity-dependent behavior observed in this study indicates the presence of an optimal ionic strength range in which silica NPs and associated surface-active agents remain well dispersed and readily adsorb at the oil-water interface, forming a compact and stable interfacial layer that promotes significant IFT reduction. Similar salinity ranges have been reported for silica-based systems (Khormali et al., 2023). In contrast, at higher salinities, the increased concentrations of cations and anions compress the electrical double layer and intensify ion-surface interactions, which can disrupt the interfacial structure and reduce electrostatic stabilization (Wen et al., 2025). Consistent with zeta-potential and aggregation studies, elevated salinity is commonly associated with decreased colloidal stability and increased effective particle size (Bijani et al., 2022; Nyah et al., 2024). As a consequence, NP aggregation and partial desorption or rearrangement of surface-active species at the oil-water interface become more likely, resulting in higher IFT values and reduced NF effectiveness (Sze Lim et al., 2023; Mumbere et al., 2025). Therefore, excessively high salinity can affect the ability of silica-based NFs to maintain ultra-low IFT, potentially limiting their overall performance in EOR applications.

The IFT between the NF solution and crude oil was also evaluated as a function of temperature and aging time to assess thermal responsiveness and temporal stability. IFT measurements conducted at elevated temperatures (up to 70 °C) showed a noticeable decrease compared to ambient conditions, dropping from 0.0288 to 0.0098 mN/m. This reduction is likely due to enhanced molecular mobility and reduced oil viscosity at higher temperature, which promote faster diffusion and more efficient adsorption of surface-active agents at the interface.

The long-term stability of the NF's interfacial activity was studied by monitoring IFT against heavy crude oil over an aging period of 1 to 45 days at reservoir temperature (40 °C) and three different salinity levels: Low (18 g/L), moderate (60 g/L), and high (200 g/L), as shown in Fig. 5.

At low salinity, the NF initially showed strong interfacial performance, achieving an IFT as low as 0.03 mN/m on day 1. However, a gradual degradation in performance was observed with prolonged aging, as the IFT increased to 2.15 mN/m after 45 days. At moderate salinity, a similar trend was observed, with the IFT increasing from 0.04 to 0.20 mN/m over the aging period. The increase in both cases may be attributed to NPs agglomeration, surfactant degradation, or changes in fluid structure over time. In contrast, under high salinity conditions the IFT values remained relatively more stable, fluctuating within a narrower range - from 0.15 mN/m on the first day to 0.24 mN/m on the final day of observation. Under high salinity conditions, the relatively stable IFT values over the aging period suggest that the NF's interfacial activity is less affected by prolonged exposure. This stability may be due to the shielding effect of the high ionic strength, which can reduce NP agglomeration by compressing the electric double layer around particles, thus maintaining better dispersion (Hassani et al., 2024). Additionally, surfactant molecules may form more robust adsorption layers at the oil-water interface in the presence of high salt concentrations, preventing rapid degradation or rearrangement. However, the initial IFT values are higher compared to low-salinity cases, likely because increased salinity reduces surfactant solubility and mobility, limiting maximum IFT reduction.

3.3 Wettability alteration of NF to carbonate rocks

Static contact angle measurements were performed on carbonate rock to evaluate the wettability alteration capability of the NF. As shown in Fig. 6, the initial water contact angle was 66.3°, indicating a water-wet surface. After aging in crude oil, the CA increased to 91.65°, confirming a transition toward an oil-wet state due to the adsorption of polar oil components - primarily resins and asphaltenes. Upon exposure to the NF, a significant wettability change was observed. After just one day of treatment with a 0.3 wt% NF solution, the CA dropped to 31.05°, and continued aging further reduced it to 29.5°, 28.8°, 16.53°, and 13.7° after 3, 6, 15, and 30 days, respectively. This transition toward a more water-wet state highlights the effectiveness of the NF in modifying surface properties, pri-

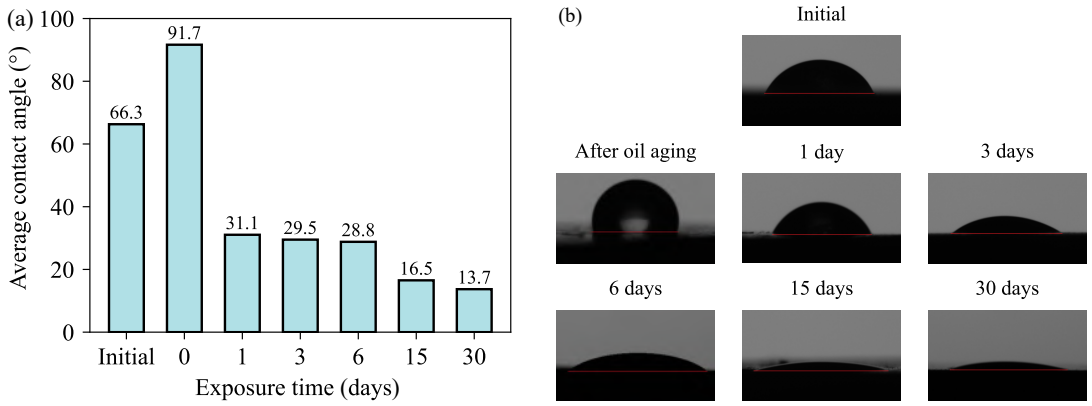

Fig. 6. Effect of aging time on wettability alteration: (a) Contact angle measurements and (b) droplet morphology.

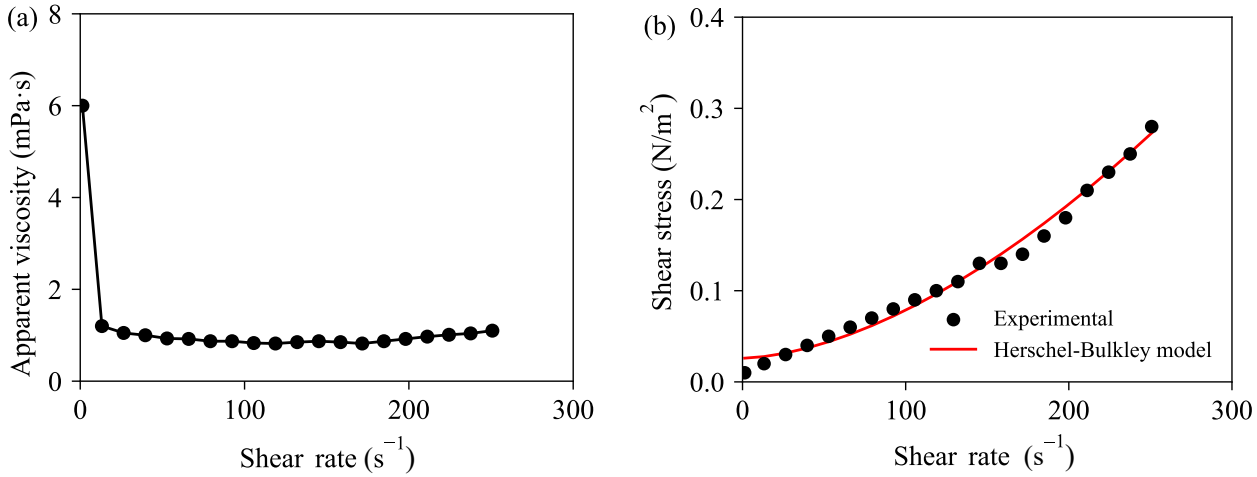

Fig. 7. (a) Apparent viscosity vs. shear rate for 0.3 wt% NF and (b) Shear stress vs. shear rate. Experimental data (black) with Herschel-Bulkley model fit (red).

marily due to the adsorption of surface-active agents and NP interactions with the adsorbed oil layer. This progressive shift toward water-wet condition demonstrates the time-dependent efficiency of the NF in altering rock wettability. Corresponding CA images clearly illustrate the transition from oil-wet to strongly water-wet conditions through visibly reduced droplet angles and increased spreading over time.

3.4 Rheological behavior of nanofluid systems

The 0.3 wt% NF solution exhibited non-Newtonian, shear-thinning behavior. As shown in Fig. 7(a), the apparent viscosity decreased sharply with increasing shear rate from 6 mPa·s at 1.32 s^{-1} to below 1 mPa·s at higher shear rates (> 50 s^{-1}), indicating pseudoplastic flow behavior. This reduction in viscosity is due to the alignment and reorganization of NPs and surface-active agents under shear, which reduces internal resistance to flow. This trend is favorable for EOR applications, where reduced viscosity under high shear promotes better injectivity, while higher viscosity at low shear helps with mobility control in porous media.

The relationship between shear stress and shear rate exhibited a nonlinear trend consistent with the Herschel-Bulkey model (Eq. (1)). As shown in Fig. 7(b), the fitting yielded a high coefficient of determination ($R^2 = 0.989$), confirming the presence of a finite yield stress and reinforcing the fluid's shear-thinning behavior:

$$\tau = 0.026 + 0.023\gamma^{1.68} \quad (1)$$

where τ is the shear stress, Pa; γ is the shear rate, s^{-1}.

In addition, viscosity decreased with increasing temperature, from approximately 1.8 mPa·s at 20 °C to 0.4 mPa·s at 70 °C, reflecting typical thermal thinning behavior that facilitates easier flow at elevated reservoir temperatures. The presence of a finite yield stress indicates that the NF requires a threshold force to initiate flow, potentially enhancing mobility control by minimizing early channeling during injection. Meanwhile, its shear-thinning behavior allows reduced viscosity under high shear rates, promoting injectability, while maintaining sufficient viscosity at low shear rates to improve displacement efficiency.

The rheology of NF-based emulsions was systematically assessed as a function of WOR and mixing time. As shown

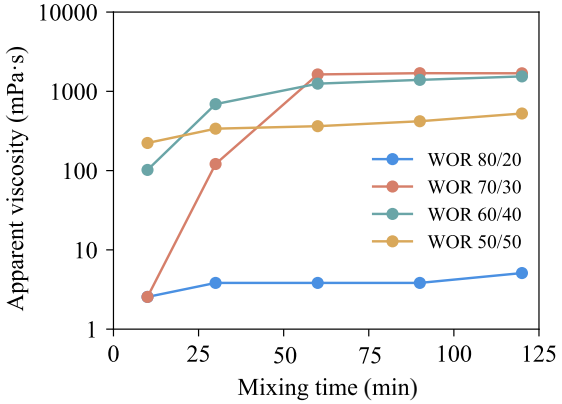

Fig. 8. Apparent viscosity of 0.3 wt% NF-based emulsions as a function of mixing time and WOR.

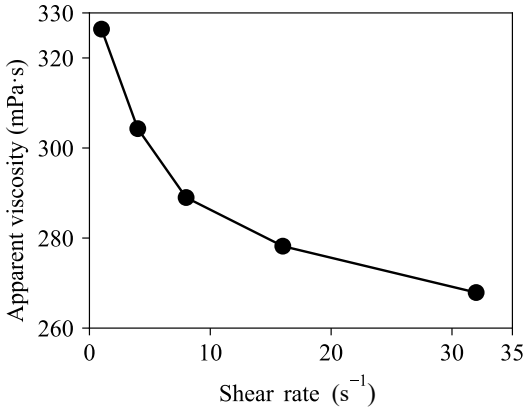

Fig. 9. Apparent viscosity vs. shear rate for the 50/50 emulsion.

in Fig. 8, emulsion viscosity increased significantly with both oil content and mixing duration, indicating composition- and time-dependent structuring. At a WOR of 80/20, viscosity remained relatively low, rising slightly from 2.55 mPa·s at 10 min to 5.1 mPa·s at 120 min, suggesting limited droplet interaction at low internal-phase fractions. In contrast, higher oil fractions caused sharp viscosity increase, particularly after 30 min of mixing. For example, at WOR of 70/30, viscosity increased dramatically from 2.55 mPa·s to 1,689 mPa·s over 120 min, reflecting rapid emulsion network formation even at moderate oil contents. Emulsions with WOR values of 60/40 and 50/50 exhibited high initial viscosities at 10 min of mixing (102 mPa·s and 223.1 mPa·s, respectively), which further increased to 1,543 mPa·s and 525.3 mPa·s after 120 min, highlighting the strong influence of both internal-phase volume fraction and mixing history.

The observed viscosity evolution can be explained by classical emulsion rheology, where emulsion viscosity is closely related to the volume fraction of the internal phase and emulsion structure, as described by the Einstein's viscosity relationship (Eq. (2)) (Du et al., 2024):

$$\mu = \frac{\mu_0}{1-(h\varphi)^{1/3}} \tag{2}$$

where μ is the relative emulsion viscosity, mPa·s; μ_0 is the viscosity of the external phase, mPa·s; φ is volume fraction of the internal phase, %; h is a parameter related to emulsion type.

As the internal phase fraction increases, the viscosity initially rises due to increased droplet concentration and restricted mobility within the continuous phase. With prolonged mixing, enhanced dispersion and adsorption of NPs and surface-active agents at the oil-water interface promote electrostatic and steric stabilization, inhibit droplet coalescence, and reduce effective droplet size, further increasing viscosity. At higher internal-phase fractions, dispersed droplets become densely packed, and interfacial adsorption layers begin to overlap, increasing osmotic pressure and resistance to droplet rearrangement. However, when the internal-phase volume exceeds a critical threshold, spatial confinement and droplet deformation can lead to partial coalescence or structural rearrangement, which may explain the non-monotonic viscosity change observed at high oil fractions. All viscosity measurements were performed at a fixed shear rate corresponding to estimated flow conditions in the target reservoir, ensuring relevance for field-scale application. The pronounced viscosity enhancement resulted in a substantial improvement in mobility control. Compared with conventional waterflooding (mobility ratio, $M \approx 67.12$), the NF-based emulsions achieved dramatically lower mobility ratios, reaching 0.043 for WOR 60/40 and 0.039 for WOR 70/30. Mobility ratios below unity are recognized as favorable for EOR, as they suppress viscous fingering and promote more uniform oil displacement (Ganat and Ali, 2024; Khlaifat et al., 2024).

For context, field-scale polymer flooding applications typically target mobility ratios well below 1 rather than unity. For example, in the Daqing oilfield, injection of a ~45 cP polymer solution to displace ~10 cP oil resulted in a mobility ratio of approximately 0.25 (Wang et al., 2008). Previous studies have shown that, for reservoirs with moderate heterogeneity and crossflow between layers, optimum sweep efficiency is achieved at mobility ratios around 0.25 rather than at unity (Dongmei et al., 2022). In this regard, the mobility ratios achieved by the NF-based emulsions in this study are lower than those typically targeted in polymer flooding, indicating strong mobility control. Unlike conventional polymer flooding, where low mobility ratios are commonly achieved through high polymer concentrations that may cause injectivity and pressure-related issues, the NF-based emulsion system attains effective mobility control through *in situ* emulsion formation and moderate viscosity enhancement.

Based on these results, NF-based emulsions are particularly suitable for post-waterflood applications when water cut is in the range of 50%-70%, enabling enhanced residual oil recovery by improving mobility control and redirecting flow into unswept, oil-rich zones. Viscosity versus shear rate data for the 50/50 WOR emulsion (Fig. 9) demonstrated shear-thinning behavior, with viscosity decreasing from 326.4 mPa·s to 267.9 mPa·s as shear rate increased from 1 to 32 s^{-1}. Although the shear rate range was limited by the viscometer's operational constraints, this confirms pseudoplastic flow typical of complex emulsions.

These results highlight the potential of NF-based emul-

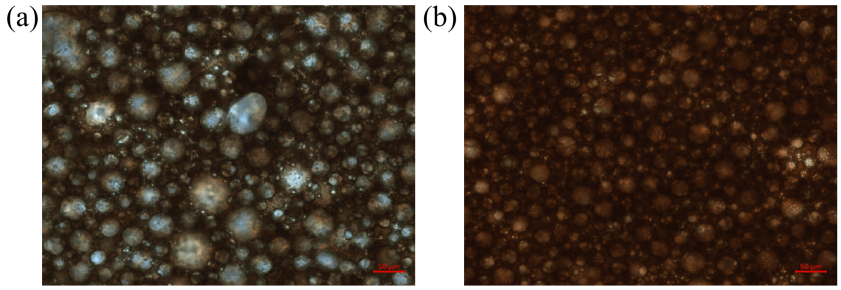

Fig. 10. Optical micrographs of 0.3 wt% NF-based emulsions at WOR (a) 50/50 and (b) 60/40.

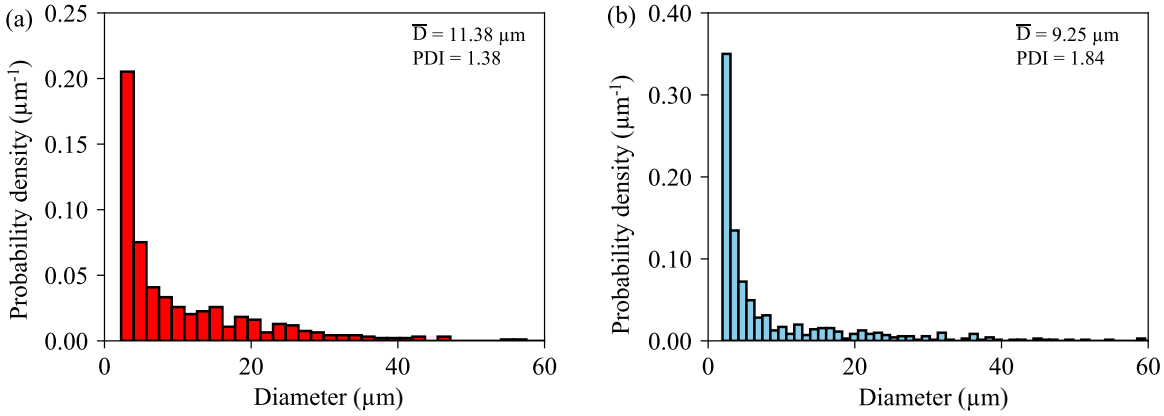

Fig. 11. Size distribution of 0.3 wt% NF-based emulsion droplets at WOR (a) 50/50 and (b) 60/40.

sions in practical EOR operations. As emulsions increase in viscosity with oil content and mixing duration, they form stable internal structures that resist deformation, improving their ability to control fluid movement in heterogeneous reservoirs. Higher viscosities improve mobility control, reducing early viscous fingering and channeling. Such stable emulsions improve sweep efficiency by diverting displacing fluids into less-swept zones, enhancing oil recovery. Furthermore, the ability to tune emulsion viscosity through WOR adjustment and mixing time offers flexibility in optimizing injection formulations for specific reservoir conditions. Additionally, shear-thinning allows emulsions to flow more easily through tight pores near the wellbore while maintaining its mobility control deeper in the reservoir. However, excessive viscosity may reduce injectability, so balancing rheological properties is critical for successful EOR implementation.

3.5 Emulsion characterization

Microscopic analysis was first conducted to investigate the morphology and type of emulsions at WOR 60/40 and 50/50, which were selected due to their best rheological performance and as a representative balanced case, respectively. The micrographs revealed the formation of complex multiple emulsions, predominantly of the water-in-oil-in-water (W/O/W) type (Fig. 10), indicating effective stabilization at both internal and external interfaces.

The presence of a polymeric structure within the continuous phase likely further contributed to this enhanced stability (Chevalier et al., 2022; Kumar et al., 2022; Zhi et al., 2023). During observation, the emulsions remained well-dispersed over an extended period, showing no signs of phase separation. Droplet size analysis, based on multiple micrographs, showed average diameters of approximately 11.4 μm for WOR 50/50 and 9.3 μm for WOR 60/40 (Fig. 11), consistent with the observed rheological behavior.

The difference in average droplet size between emulsions reflects the influence of WOR on emulsion microstructure and stability. These complex W/O/W emulsions contain smaller internal droplets dispersed within larger external droplets. These measurements focused on the size of the larger, external droplets, which showed a right-skewed distribution for both WORs, indicating the presence of many smaller droplets and fewer large droplets. The droplet size distribution was moderately polydisperse and skewed, with PDI values of 1.38 for 50/50 and 1.84 for 60/40. Despite this non-uniformity, the emulsions maintained well-defined internal structures and demonstrated good stability without rapid coalescence. At WOR 60/40, the higher oil fraction favors the formation of smaller external droplets due to increased NP stabilization and interfacial area, resulting in a finer dispersion. Conversely, at WOR 50/50, closer to equal volumes of water and oil, the external droplets tend to be larger, possibly due to greater coalescence and less efficient stabilization. The broader size distribution and higher polydispersity observed at WOR 50/50 further highlight the complexity of the emulsion structure. This heterogeneity can affect rheological behavior and emulsion stability, both of which are crucial for mobility control and

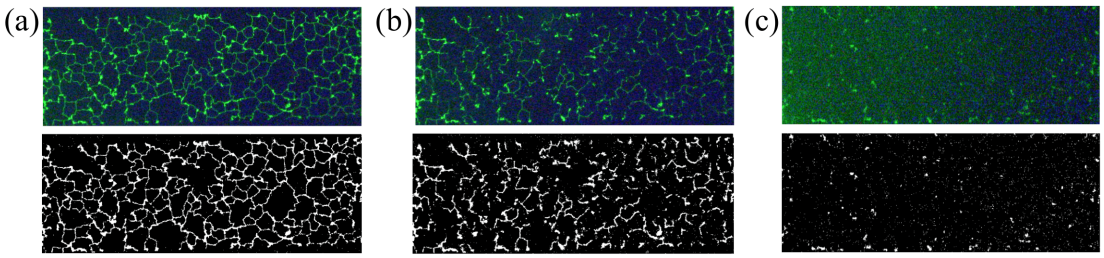

Fig. 12. Fluorescence (left) and binarized (right) micrographs of oil distribution in microfluidic chip at different stages: (a) Initial state with 100% oil saturation, (b) after waterflooding and (c) after NF flooding.

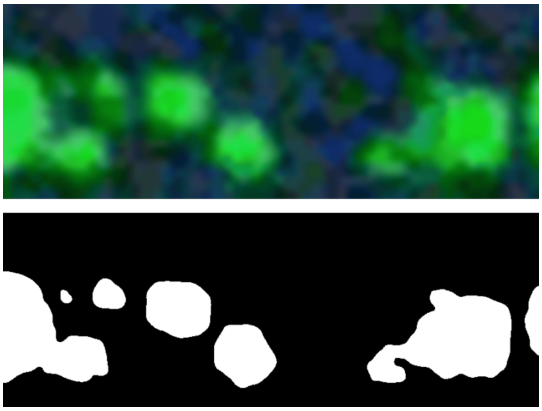

Fig. 13. Fluorescence and binarized micrographs of oil droplets at the outlet of the microfluidic chip during the NF flooding stage.

sweep efficiency in EOR processes. By adjusting the WOR, it is possible to tailor the droplet size and distribution, thereby optimizing emulsion performance under reservoir conditions.

3.6 Microfluidic test

To evaluate the oil displacement performance of the NF-based emulsions, microfluidic flooding experiments were conducted and visualized using fluorescence microscopy. First, the microfluidic chip was saturated with crude oil. The fluorescence image of the chip fully saturated with the hydrocarbon phase, along with the corresponding binarized image, is presented in Fig. 12(a). A baseline displacement test was conducted using brine to evaluate the effectiveness of subsequent NF injection. As illustrated in Fig. 12(b), waterflooding resulted in a recovery factor of 30.19%, with significant volumes of oil remaining trapped in unswept regions of the pore network due to unfavorable mobility ratio and channeling effects.

Following waterflooding, the NF was injected to evaluate its EOR potential and *in situ* emulsion formation behavior. The fluorescence and binarized images obtained after NF injection (Fig. 12(c)) show a substantial reduction in residual oil saturation, despite minor image noise caused by light scattering. Image-based analysis indicates that the recovery factor increased to 70.93%, demonstrating a markedly improved displacement efficiency compared to brine flooding. During NF injection, a pronounced increase in pressure was observed, reflecting increased flow resistance within the porous medium. This pressure response, together with visual observations, is indicative of *in situ* emulsion formation and enhanced mobility control. Direct quantitative measurement of emulsion droplet size and distribution within the micromodel was not feasible due to optical resolution limitations and the highly dynamic nature of emulsification in confined pore geometries. Instead, emulsion formation was qualitatively confirmed by the appearance of well-defined, spherical oil droplets collected at the chip outlet (Fig. 13), which are characteristic of stabilized emulsified oil dispersed in the aqueous phase.

While NF-based emulsions exhibit strong mobility control and interfacial activity at the laboratory scale, their long-term behavior under continuous field injection requires careful evaluation. Prolonged injection of viscous emulsions or *in situ*-generated droplets can cause pressure buildup, partial pore-throat restriction, and even permeability impairment if droplet accumulation and retention are not controlled (Santos et al., 2023). In particular, sustained injection of NP-stabilized emulsions can increase flow resistance in high permeability channels, leading to stepwise rises in injection pressure and localized injectivity loss. At the pore scale, accumulation of emulsion droplets within larger pores and throats can alter flow paths and redistribute injected fluids. While such behavior may enhance sweep efficiency by diverting flow into previously unswept regions, excessive retention can also reduce effective permeability and hinder long-term injectivity (Hu et al., 2023). These risks can be mitigated by careful formulation design and operational control. Tuning NP surface (for example, silica or magnetic NPs with tailored wettability or polymer/surfactant coatings) can improve colloidal stability while limiting irreversible aggregation and retention in porous media. In addition, adjusting key formulation parameters, including NP concentration, WOR, and brine salinity, allows control over emulsion viscosity and droplet size distribution, thereby reducing excessive pressure gradients while maintaining effective mobility control (Qin et al., 2020). Injection strategy also plays a key role in minimizing long-term impairment. Staged or slug-based injection schemes, as well as alternating emulsion-brine cycles, can limit continuous droplet accumulation and mitigate pore blockage while preserving profile-control benefits. Periodic waterflooding between emulsion slugs can help re-mobilize retained droplets and stabilize injection pressures. Finally, integrated pre-screening workflows are critical prior to field application. Combined rheological measurements and pore-scale displacement tests in microfluidic models or core

plugs enable identification of operational windows where viscosity enhancement, droplet transport, and pressure response remain compatible with injectivity constraints. Such integrated laboratory evaluations provide essential guidance for scaling NF-based emulsion formulations and injection strategies from laboratory studies to reliable field-scale implementation.

4. Conclusions

In this study, the behavior and performance of NF-based cEOR were systematically evaluated through rheological analysis, interfacial property measurements, emulsion characterization, and microfluidic displacement test. The results demonstrate strong potential of this approach to improve oil recovery under reservoir-relevant conditions. Key findings include:

1) Enhanced mobility control: NF-based emulsions exhibited tunable viscosity and shear-thinning behavior. Their mobility ratios ($M \approx 0.039 - 0.043$) were far below that of waterflooding ($M \approx 67$), enabling better control of flow profiles and sweep efficiency.
2) Significant IFT reduction: The NF formulations reduced the oil-brine IFT from 29.7 mN/m to 0.029 mN/m, facilitating easier droplet formation and emulsification, which supports improved displacement efficiency.
3) Wettability alteration: Contact angle measurements showed a reduction from 91.65° to 13.70°, indicating wettability alteration that favors water wetting of the rock surface.
4) Structurally stable emulsions: Microscopy revealed complex W/O/W emulsion morphology, with distinct internal structures and moderate polydispersity. Emulsions showed no signs of rapid coalescence, indicating satisfactory stability.
5) Effective oil displacement: Microfluidic tests demonstrated significant mobilization of residual oil left after waterflooding. The overall increase in recovery and visible oil mobilization confirmed the emulsion's *in situ* effectiveness. Discrete oil-in-water droplets were observed at the microchip outlet, along with a pressure increase during injection. This confirms *in situ* emulsion formation, which aids flow diversion and oil recovery.

Based on this study's findings, future work will focus on optimizing emulsion formulations to balance viscosity, injectivity, and stability for specific reservoir conditions such as temperature, salinity, and heterogeneity. Long-term stability tests under high-pressure, high-temperature conditions are needed to assess performance over extended periods. Core flooding experiments will validate lab results under real conditions. Additionally, molecular dynamics simulations and hydrodynamic modeling will be used to better predict emulsion behavior, fluid-surface interactions, and optimize flooding performance across multiple scales – from molecular to core to field.

Acknowledgements

The authors acknowledge the support from the Ministry of Science and Higher Education of the Russian Federation under agreement No. 07515-2022-299 within the framework of the development program for a world-class Research Center "Efficient development of the global liquid hydrocarbon reserves".

Additional information: Author's email

megycd@163.com (C. Yuan)

Conflicts of interest

The authors declare no competing interest.

References

Alnarabiji, M. S., Yahya, N., Nadeem, S., et al. Nanofluid enhanced oil recovery using induced ZnO nanocrystals by electromagnetic energy: Viscosity increment. Fuel, 2018, 233: 632-643.

Behera, U. S., Poddar, S., Deshmukh, M. P., et al. Comprehensive review on the role of nanoparticles and nanofluids in chemical enhanced oil recovery: Interfacial phenomenon, compatibility, scalability, and economic viability. Energy and Fuels, 2024, 38(15): 13760-13795.

Bijani, M., Khamehchi, E., Shabani, M. Comprehensive experimental investigation of the effective parameters on stability of silica nanoparticles during low salinity water flooding with minimum scale deposition into sandstone reservoirs. Scientific Reports, 2022, 12(1): 16472.

Chevalier, R. C., Gomes, A., Cunha, R. L. Role of aqueous phase composition and hydrophilic emulsifier type on the stability of W/O/W emulsions. Food Research International, 2022, 156: 111123.

Dongmei, W., Namie, S., Seright, R. Pressure modification or barrier issues during polymer flooding enhanced oil recovery. Geofluids, 2022, 2022: 6740531.

Dorhjie, D. B., Pereponov, D., Aminev, T., et al. A microfluidic and numerical analysis of non-equilibrium phase behavior of gas condensates. Scientific Reports, 2024, 14(1): 9500.

Du, D., Hou, S., Pu, W., et al. Investigation on enhanced oil recovery potential of active nano-SiO_2 in high-temperature and high-salinity reservoirs at core and pore scale. Fuel, 2026, 404: 136363.

Du, D., Li, J., Pu, W., et al. Experimental study on EOR potential of *in-situ* water in oil emulsion in low-temperature conglomerate reservoirs. Geoenergy Science and Engineering, 2024, 241: 213097.

Filippov, S. K., Khusnutdinov, R., Murmiliuk, A., et al. Dynamic light scattering and transmission electron microscopy in drug delivery: A roadmap for correct characterization of nanoparticles and interpretation of results. Materials Horizons, 2023, 10(12): 5354-5370.

Ganat, T., Ali, I. Mobility control requirement in EOR processes, in Advancements in Chemical Enhanced Oil Recovery, edited by T. Sharma, K. R. Chaturvedi, T.

Ganat and I. Ali, Apple Academic Press, Palm Bay, pp. 225-244, 2024.

Gong, Y., Li, L., Huang, W., et al. A study of alkali-silica nanoparticle-polymer (ANP) flooding for enhancing heavy oil recovery. Journal of Petroleum Science and Engineering, 2022, 213: 110465.

Hassani, K., Zheng, W., Rostami, B. Rock wettability and interfacial tension improvement by exposure time effect in modified water injection process coupled with silica nanoparticles. Petroleum Science and Technology, 2024, 42(9): 1031-1046.

Hu, X., Long, Y., Xuan, G., et al. Optimized hydrophobic magnetic nanoparticles stabilized Pickering emulsion for enhanced oil recovery in complex porous media of reservoir. Frontiers in Energy Research, 2023, 11:1212664.

Jang, H., Lee, W. S., Lee, J. Performance evaluation of surface-modified silica nanoparticles for enhanced oil recovery in carbonate reservoirs. Colloids and Surfaces A: Physicochemical and Engineering Aspects, 2024, 681: 132784.

Karambeigi, M. S., Abbassi, R., Roayaei, E., et al. Emulsion flooding for enhanced oil recovery: Interactive optimization of phase behavior, microvisual and core-flood experiments. Journal of Industrial and Engineering Chemistry, 2015, 29: 382-391.

Khlaifat, A. L., Fakher, S., Harrison, G. H. Evaluating factors impacting polymer flooding in hydrocarbon reservoirs: Laboratory and field-scale applications. Polymers, 2024, 16(1): 75.

Khormali, A., Koochi, M. R., Varfolomeev, M. A., et al. Experimental study of the low salinity water injection process in the presence of scale inhibitor and various nanoparticles. Journal of Petroleum Exploration and Production Technology, 2023, 13(3): 903-916.

Kumar, A., Kaur, R., Kumar, V., et al. New insights into water-in-oil-in-water (W/O/W) double emulsions: Properties, fabrication, instability mechanism, and food applications. Trends in Food Science and Technology, 2022, 128: 22-37.

Liu, R., Deng, J., Pu, W., et al. Micro- and macroscopic experiments on self-adaptive mobility control and displacement efficiency of carbon-based composite nanofluid for enhanced oil recovery. Petroleum, 2025, 11(2): 211-225.

Lu, Z., Wang, L., Guo, Z., et al. The microfluidic in geo-energy resources: Current advances and future perspectives. Advances in Geo-Energy Research, 2025, 16(2): 171-180.

Mansouri Zadeh, M., Amiri, F., Hosseni, S., et al. Synthesis of colloidal silica nanofluid and assessment of its impact on interfacial tension and wettability for enhanced oil recovery. Scientific Reports, 2024, 14(1): 325.

Mumbere, W., Sagala, F., Gupta, U., et al. Reservoir potential unlocked: Synergies between low-salinity water flooding, nanoparticles and surfactants in enhanced oil recovery - A review. ACS Omega, 2025, 10(29): 31216-31261.

Nyah, F., Ridzuan, N., Ikechukwu Nwaichi, P., et al. Comprehensive review on the role of salinity on oil recovery mechanisms during chemical flooding. Journal of Molecular Liquids, 2024, 415: 126308.

Pang, Q., Pu, W., Tang, X., et al. Experimental investigation and simulation of W/O emulsion flow in nanofluid flood for enhanced oil recovery. Geoenergy Science and Engineering, 2024, 239: 212973.

Pu, W., He, Y., Liu, R., et al. Functionalized silica nanoparticles for enhanced heavy oil recovery: Experiment and molecular dynamics simulation. Energy and Fuels, 2025, 39(29): 14055-14069.

Qin, T., Goual, L., Piri, M., et al. Nanoparticle-stabilized microemulsions for enhanced oil recovery from heterogeneous rocks. Fuel, 2020, 274: 117830.

Santos, L. B. L., Silva, A. C. M., Pereira, K. R. O., et al. Microemulsions stabilized with nanoparticles for EOR: A review. Journal of Molecular Liquids, 2023, 391: 123271.

Sepahvand, M., Ghalenavi, H., Salari Goharrizi, F., et al. Integrating low salinity water, surfactant solution, and functionalized magnetite nanoparticles with natural acidic groups for enhanced oil recovery: Interfacial tension study. Journal of Molecular Liquids, 2024, 405: 124944.

Shakeel, M., Sagandykova, D., Mukhtarov, A., et al. Maximizing oil recovery: Innovative chemical EOR solutions for residual oil mobilization in Kazakhstan's waterflooded sandstone oilfield. Heliyon, 2024, 10(7): e28915.

Souza, T. G. F., Ciminelli, V. S. T., Mohallem, N. D. S. A comparison of TEM and DLS methods to characterize size distribution of ceramic nanoparticles. Journal of Physics: Conference Series, 2016, 733(1): 012039.

Sze Lim, S. S., Elochukwu, H., Nandong, J., et al. A review on the mechanisms of low salinity water/surfactant/nanoparticles and the potential synergistic application for c-EOR. Petroleum Research, 2023, 8(3): 324-337.

Wang, D., Han, P., Shao, Z., et al. Sweep-improvement options for the Daqing Oil Field. SPE Reservoir Evaluation and Engineering, 2008, 11(1): 18-26.

Wen, Y., Zhang, C., Zhu, G., et al. Combined effects of nanofluid and surfactant on enhanced oil recovery: An experimental study. ACS Omega, 2025, 10(44): 52375-52386.

Wu, H., Chang, J., Xu, G., et al. In-situ emulsification and viscosification system of surfactant-assisted Janus nanofluid and its profile control effect. Advances in Geo-Energy Research, 2024, 14(2): 135-146.

Yang, L., Ge, J., Wu, H., et al. Study on the enhanced oil recovery properties of the pickering emulsions for harsh reservoirs. ACS Omega, 2024, 9(49): 48427-48437.

Zhi, Z., Liu, R., Wang, W., et al. Recent progress in oil-in-water-in-oil (O/W/O) double emulsions. Critical Reviews in Food Science and Nutrition, 2023, 63(23): 6196-6207.